Digest Journal of Nanomaterials and Biostructures Vol. 20, No. 4, October-December 2025, p. 1447-1456

Fabrication of MGO: SNO_2 nanoparticles for environmental gas sensing applications

A. A. Kamil [a], R. M. Abdullah [a], R. Sedeeq [a], L. F. Hassan [a], J. Al-Khalidi [a,*], W. H. Albanda [b]
[a] *Department of Physics, College of Science, University of Diyala, Iraq*
[b] *Science Department - College of Basic Education, Mustansiriyah University, Iraq*

The structures proprieties were investigated through X-ray diffraction. The tin oxide has a constant tetragonal structure with mixing MgO, while, the grain size decreases from (35.42 nm) to (14.11 nm); FE-SEM reveals the shape and dimensions of the sample. Hall Effect measurement identifies the n-type electrical conductivity for the MgO, SnO_2, and MgO: SnO2 films, the mobility of carriers decreases when the mixing ratio increase. The sensor structures for MgO, SnO_2, and MgO: SnO2 have a high resistance in air to NH3 and CO_2 gas; the maximum ~22 sensor response at room temperature showed about 868.48 ppm of NH_3 gas for MgO: SnO_2 nanoparticles, with a fast response time of 25 s. However, the recovery time values were consistently higher than the response time values.

(Received August 25, 2025; Accepted November 13, 2025)

Keywords: MgO: SnO_2, Nanoparticles, Gas sensor, Pollutant concentration

1. Introduction

Air quality is a significant global concern. Ensuring a clean air supply is crucial for the well-being of humans and the environment; therefore, reducing environmental pollution and managing disasters effectively are necessary. Gas sensors tool is important to achieve these goals, which are capable of detecting contaminated gases concentrations. To adapt and mitigate the pollution risk, these detectors play a vital role in monitoring air quality by detecting and measuring pollutant gases to protect the ecosystem [1]. Ammonia (NH3) is an essential raw material used in many industrial factories, but it's extremely harmful to human life, especially the respiratory system [2], Therefore, it's very important to develop highly selective and sensitive gas sensors for NH3 [3]. The Sensitivity, Selectivity, and Stability are the main parameters that must be developed in gas sensors [4-6]. CO2 gas sensors are commonly used in agriculture and industrial factories to detect the air quality and identify the pollutants in the atmosphere [7, 8]. The nanoscale materials are used in gas sensor to detect the small pollutant concentrations (ex. ppb range) that instead the microelectronic due to their limitation in sensitivity [8-10]. By using varios techniques, many studeis have identfy various metal oxide nanostructures, including MgO. Several synthesis techniques are used to create MgO nanoparticles [10-15]. MgO and SnO2 are sensing materials used to increase the dispersion of the active component specially MgO is commonly used due to its stability, low cost, and high Lewis basicity for CO2 adsorption [16-17]. SnO2 nanoparticles are used widely as sensing material for fabricating gas sensors to detect C2H5OH, ammonia (NH3), H2, CH4, and H2O [18-19]. Thin films with small grain size indicate an increased surface-to-volume ratio, carrier concentration, and higher catalytic activity, which enables them to interact with a larger number of gas molecules [20-21]. SnO_2, a semiconducting material with a broadband gap and of the n-type, is highly prevalent in the gas sensor business. Commercial Taguchi gas sensors have been predominantly designed using SnO_2 since 1968. A thin film of SnO_2, deposited via RF sputtering, displayed an uneven and porous micro surface, this films detectable reaction to 1 ppm of NO_2 gas when tested at temperature 100 °C due to the abundance of accessible Sn sites on the porous surface, which is influenced by the rate of development during oxygen ion deposition and adsorption [22-23]. Researchers created doped SnO2 films and catalytic coatings to solve the issue of weak reactivity between the very stable CO2 gas

* Corresponding author: jasim_mo@uodiyala.edu.iq
https://doi.org/10.15251/DJNB.2025.204.1447

and the pure SnO2 metal oxide sheet [24, 25]. The aims of this study are creating and developing a sensing materials to detect the tiny pollutant concentration.

2. Experimental Part

The Preparation of MgO (1-x): SnO2(x) Nanoparticles including the weigh the quantities of Magnesium and tin chloride individually and dissolve each quantities in deionized water. by magnetic stirrer we mixing the two mixtures gradually with continuously moving and then adding the ammonium hydroxide solution to the blend until the pH level reaches approximately 9, to ensure guarantee that the nanoparticles completely precipitate stirring the blend continuously for 2-3 hours, when the blend pointed to white color the precipitate of MgO1-x: SnO2 (x) nanoparticles will form, by using an oven at (200°C) for 6 h the precipitates dried, the dried precipitates are subjected to thermal treatment in the furnace at (800°C) for 4 h.

Preparation of MgO, SnO2, and MgO: SnO2 nanoparticles at room temperature by dissolving them in deionized water. With a mass ratio of 0.25:10. The drop-casting approach was employed to apply a layer of MgO: SnO2 onto a silicon substrate. This was done by carefully depositing drops of a solution onto the substrate using a pipette. Prior to this, the silicon substrate was cleaned using a diluted purifier solution to eliminate any impurities and organic substances present on its surface. The study utilised pure samples of MgO and SnO2, as well as samples of MgO (0.25): SnO2 (0.25), to investigate the materials' performance in gas sensing tests.

3. Results and Discussion

In order to emphasize the crystal structure properties for the pure and blend nanoparticles XRD test was applied. XRD patterns obtained from the produced samples, the peaks observed at (2Θ = 36.98°, 42.97°, 62.39°, 74.8°, and 78.75°) corresponding to the crystalline planes indicate a cubic MgO structure (Fig.1). The space group is (Fm-3m no. 225), with lattice parameters (a=b=c= 4.2060 A°) and ($\alpha=\beta=\gamma=90°$), which closely match the standard data (JCPDS 98-016-9450). The peaks observed at specific angles (2Θ = 26.59°, 33.89°, 37.96°, 51.79°, 54.77°, 57.85°, 61.9°, 64.77°, 65.99°, 71.31°, and 78.74°) can be attributed to the planes of the Cassiterite tetragonal SnO_2 structure. This structure belongs to the space group (P42/mm no.136) and has lattice parameters (a = b = 4.7360 A° and c = 3.1850 A°) with angles ($\alpha = \beta = \gamma = 90°$). These results are consisted with the standard data (JCPDS 98-003-9173). The purity of MgO and SnO_2 is demonstrated in Fig (1).

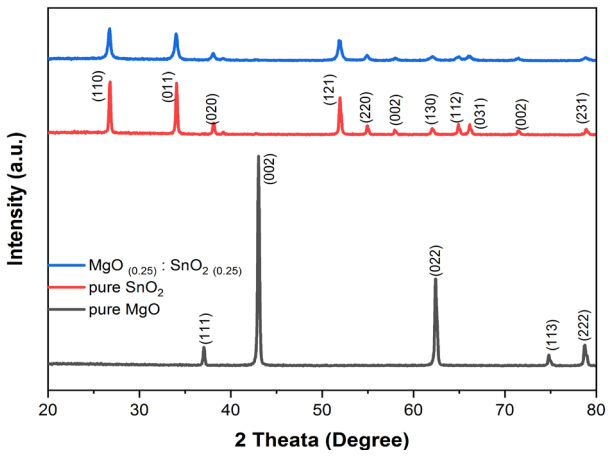

Fig. 1. XRD patterns of synthesized samples.

The XRD analysis investigate a highly pure crystalline structure in the synthesized nanoparticles, without impurity peaks. The results for MgO doping identify that the crystal structure of SnO2 unchanged for all MgO (0.5 gm) ratios, that refer to successfully link of Mg ions were into the SnO2 crystalline lattice. The resulting nanoparticles exhibited a cassiterite tetragonal structure, characteristic of pure MgO, with a space group of P42/mnm (no. 136). The XRD patterns revealed

a decrease in the intensity of the peaks of pure SnO_2 as the mixing ratio increased. Additionally, the full width half-maximum value (FWHM) increased, indicating a decrease in the crystalline growth of SnO_2 due to the presence of Mg ions. This is supported by the smaller diameter of Mg ions (0.067 nm) compared to tin ions (0.071 nm) [26, 27], as shown in Fig (1).

The diameters of the crystals of pure MgO, SnO_2, and SnO_2 doped with varied ratios (0.5, 0.6, 0.7, and 0.8 wt. %) of Mg ions were determined by calculating the strongest XRD peak using Debye Scherer's equation. The computed sizes were 24.5 nm, 35.42 nm, and 14.11 nm, respectively. The results demonstrated a distinct reduction in the size of the crystals when the ratio of Mg ions used for doping was increased. This can be attributed to the disparity in the sizes of Sn and Mg ions .[28,29]

3.1. FE-SEM Measurements

To confirm the XRD results, the FE-SEM measurements are used, including pictures and particle size distributions of the processed samples. In all samples, the synthesized nanoparticles displayed semi-spherical shapes as pointed in Fig 2 (a, b, c), they indicated that the average particle size of pure MgO was approximately 117.93 nm. In contrast, pure SnO2 nanoparticles had a smaller average particle size of 90.07 nm Fig 2 (a, b).

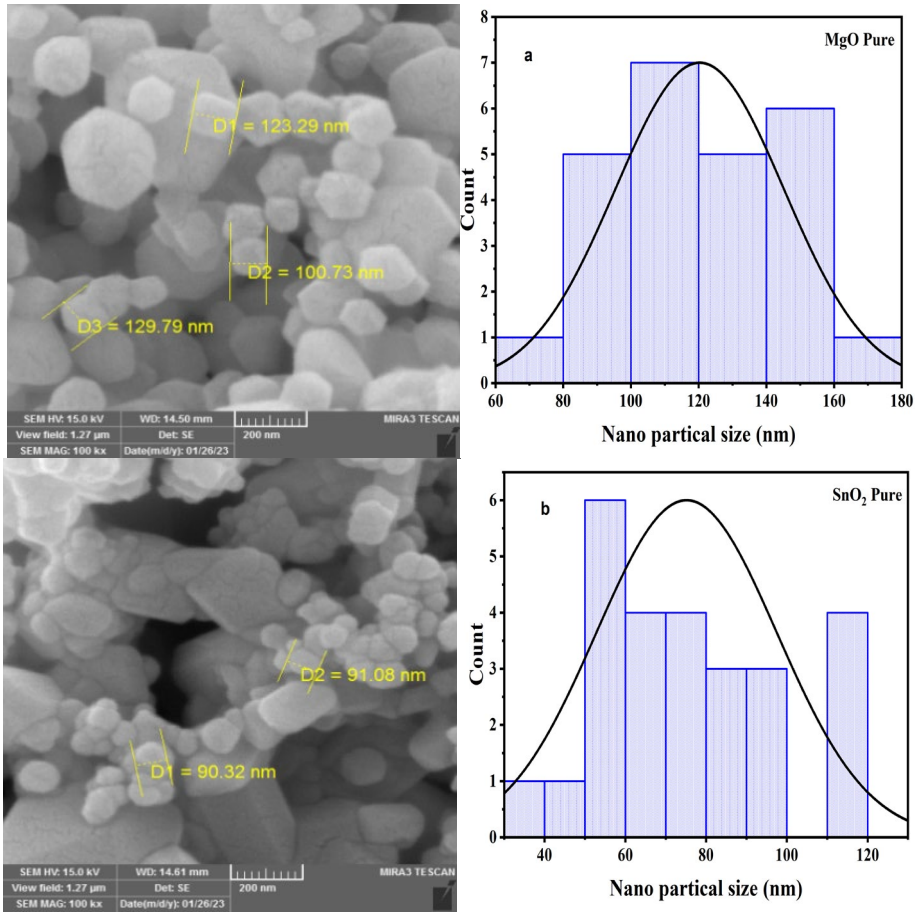

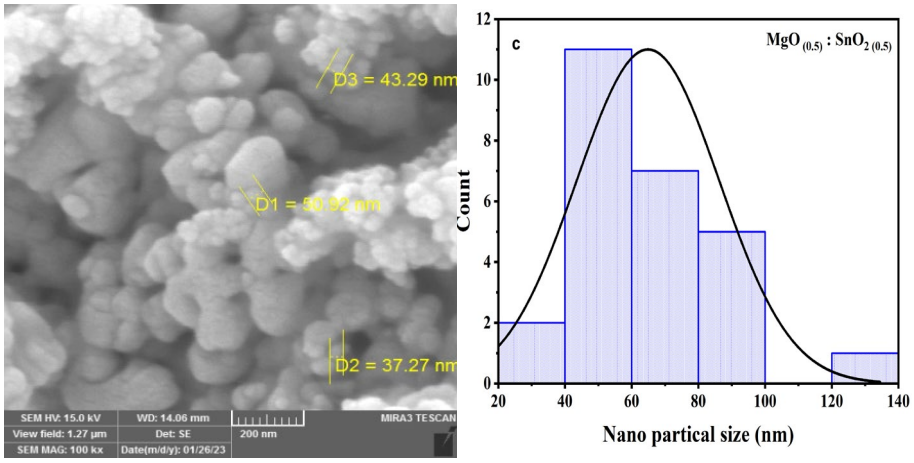

Fig. 2. FE-SEM images and particle size distribution of samples.

The FE-SEM images identify that the SnO2 nanoparticles were nearly identical in size. Figure 2(c) displayed the morphology of MgO nanoparticles combined with varying ratios of SnO2. FE-SEM pictures indicated the clustering of doped nanoparticles, which exhibited a semi-spherical shape. The MgO: SnO2 nanoparticles formed clusters. The FE-SEM image confirmed that the average particle size dropped noticeably when mixed with SnO2 due to the smaller ionic radius of Sn ions in comparison to Mg ions [30, 31].

3.2. Hall Effect Measurements

Hall Effect was applied to identify the electrical properties, it indicate that the conductivity is n-type, as the Hall coefficient signal is negative, the n-type charge carrier is due to a deficiency of oxygen atoms in the crystal structure [32, 33]. This means that electrons are the majority charge carriers, while the minority charge carriers are holes; defects in the film restrict the movement of electrons, resulting in increased resistance and making it an n-type semiconductor with low concentration. These findings align with the previous study's results [34, 35]. The observed increase in resistivity in the MgO: SnO_2 films can be attributed to an increase in disorder, the presence of the amorphous phase, and carrier scattering at grain boundaries. Another potential explanation for the rise in resistivity is the replacement of Sn^{4+} sites with Mg^{2+} ions, resulting in a reduction in carrier concentration due to carrier traps. In addition, the mobility of carriers reduces as the doping level increases due to a decrease in particle size and an increase in impurity scattering, as stated in references [36, 37].

Table 1. Hall Effect parameters for the MgO: SnO_2 thin films.

Sample	Concentration $(cm)^{-3}$	Hall Coefficient R_H (m^2/C)	Conductivity $(\Omega.cm)^{-1}$	Resistivity $(\Omega.cm)$	Mobility $(cm^2/v.s)$
MgO	-1.39	-4.49	1.70	6.04	7.62
SnO_2	-7.09	-8.80	1.65	5.90	1.46
$MgO_{(0.5)}$: $SnO_{2\,(0.5)}$	-5.93	-1.05	1.11	9.03	1.17

3.3. Gas Sensing Measurements

The films of MgO, SnO_2 pure, and MgO: SnO_2 were sequentially subjected to reductive gas (NH3) and oxidizing gas (CO2) at operating temperatures of (RT, 100, 200) °C. This section presents a concise overview of the response to each analytic and sample depicted in Figs 3, 4, and 5. These figures illustrate the changes in resistance over time when the examined gases (NH_3 and CO_2) are introduced and removed for the films of nanoparticles. The deposited films on a glass substrate are tested at different (room temperature, 100°C, and 200°C) temperatures. Adsorption of reducing

gases on the gas sensor's surface results in the transfer of electrons from the n-type samples, causing a reduction in sample resistance. A sample's resistivity decreases exponentially when exposed to NH_3 gas. This is due to the rise in the concentration of majority charge carriers in the conduction band, which enhances electrical conductivity. This finding aligns with the outcomes the Ato et al. [38] and Deshpande et al. [39] documented. On the other hand, when a sample is subjected to CO_2 gas, it absorbs additional electrons from the sample's surface, elevating its resistance. The reduction in electron concentration near the surface of the n-type semiconductor leads to an increase in the resistance of the sample. The sensitivity of the gas sensor is significantly affected by the size of the nanoparticles since a larger surface-to-volume ratio results in increased sensitivity. This phenomenon has been documented in prior research, such as the study conducted by reference [40].

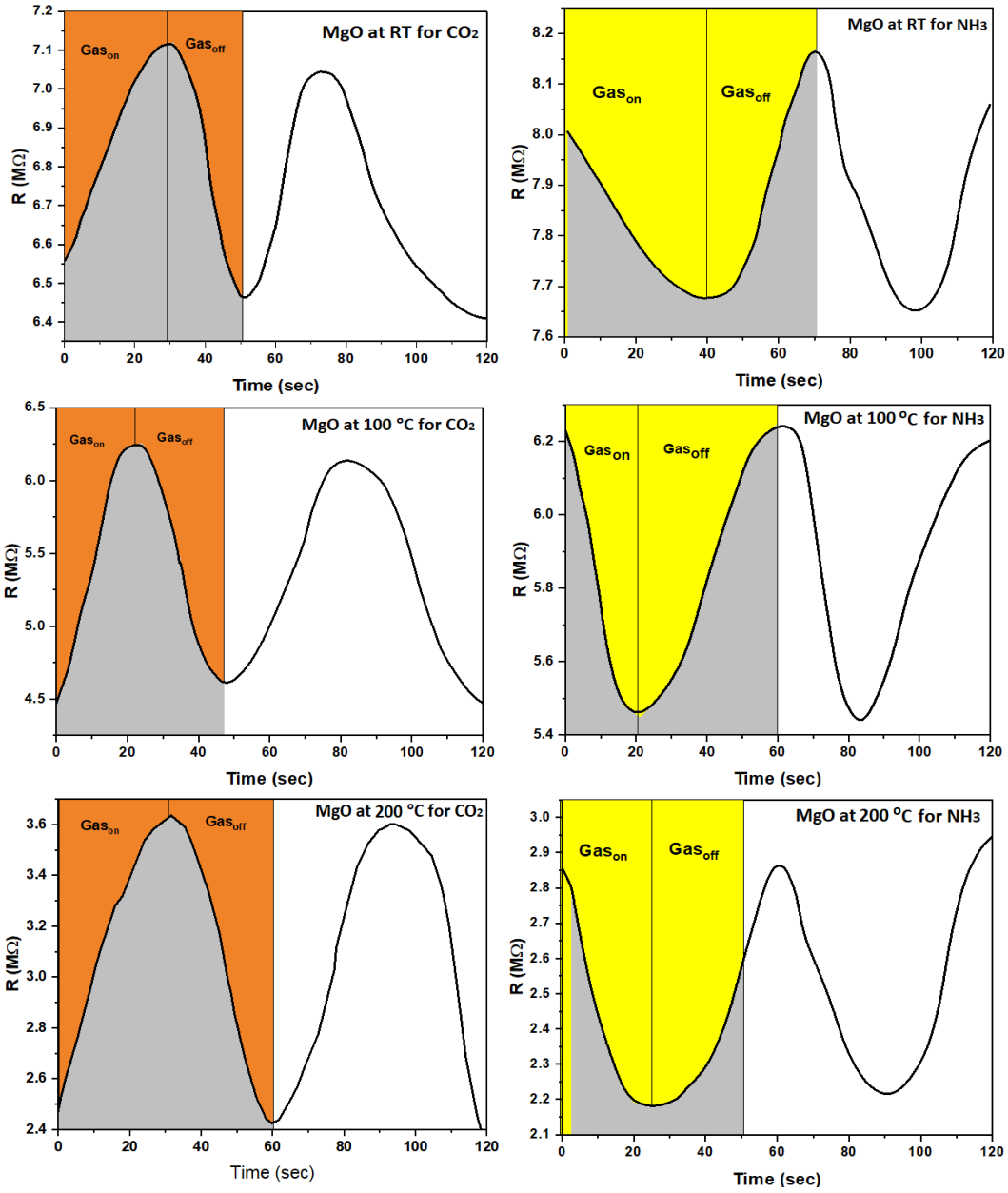

Fig. 3. Resistance variation for MgO Nanoparticles against NH_3 and CO_2 gases.

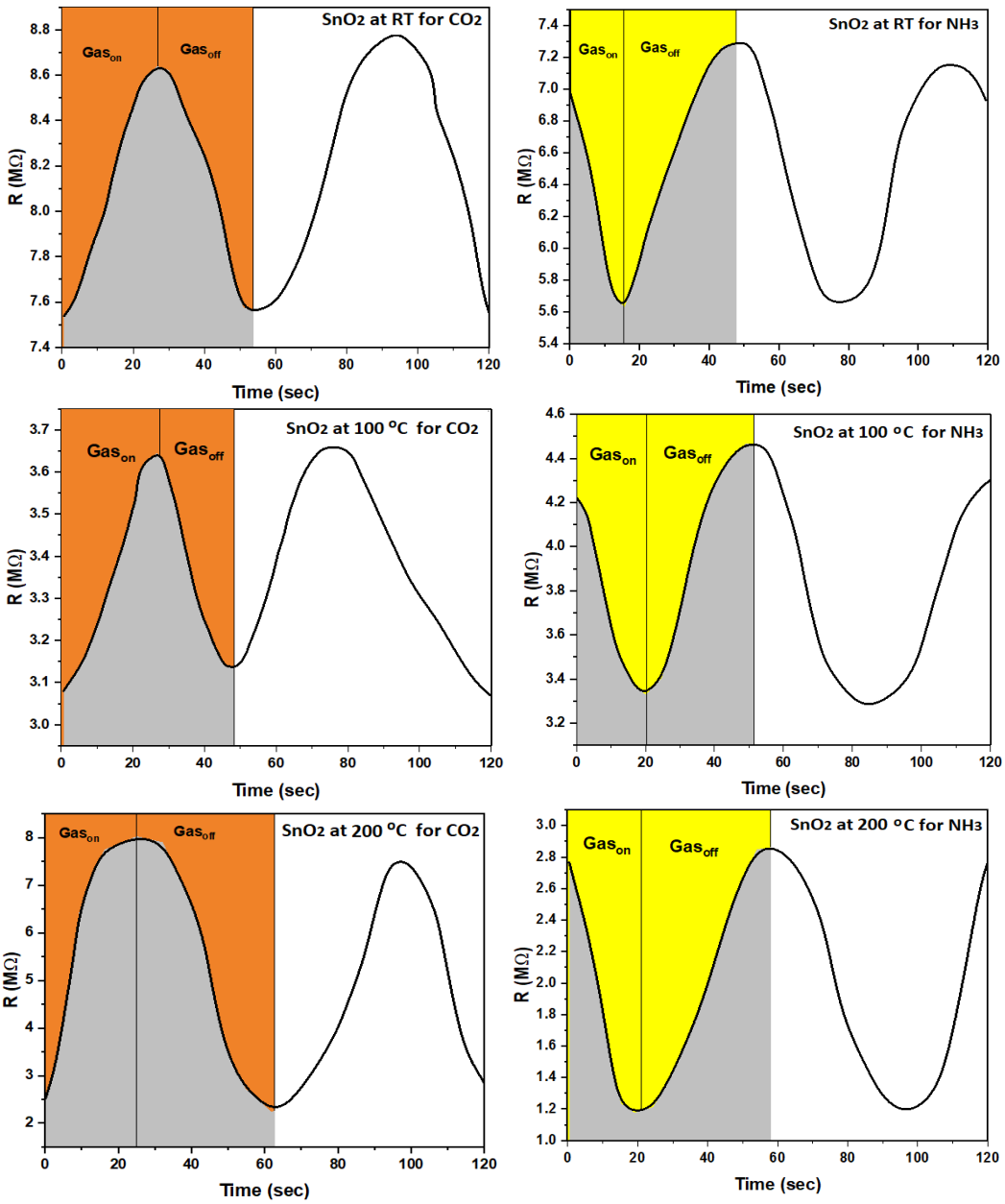

Fig. 4. Resistance variation for SnO_2 Nanoparticles against NH_3 and CO_2 gases.

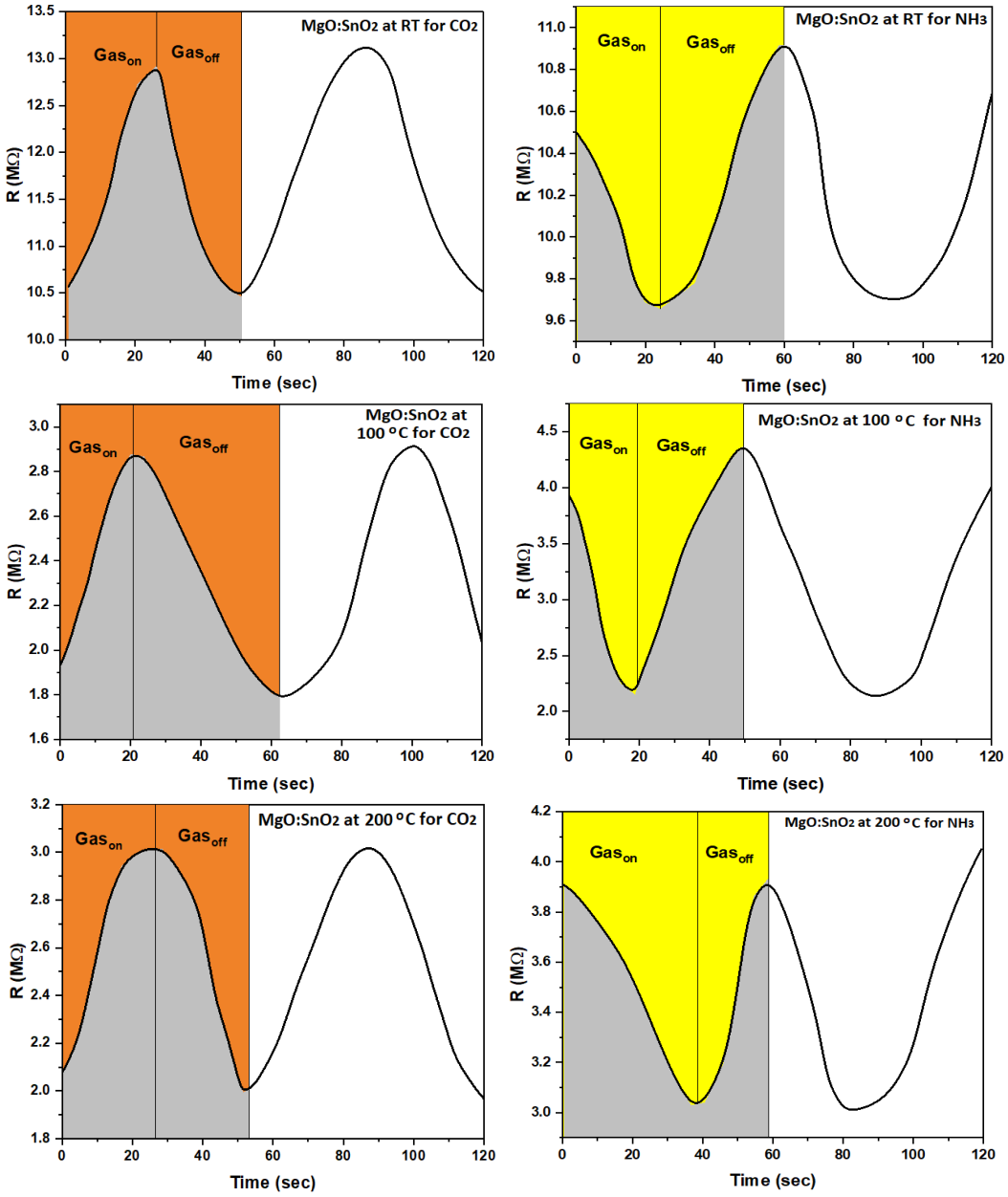

Fig. 5. Resistance variation for MgO $_{(0.25)}$:SnO$_2$ $_{(0.25)}$ Nanoparticles against NH$_3$ and CO$_2$ gases.

The changes in the response of the NH3 sensor when using pure ratio of MgO, SnO_2, and MgO $_{(0.5)}$: SnO_2 $_{(0.5)}$ thin films at various temperatures ranging from room temperature to 200 °C Fig 6. The sensor responses of MgO $_{(0.5)}$: SnO_2 $_{(0.5)}$ samples have shown an improvement compared to the pristine film's sensor response. Oxygen adsorption and desorption have a sequential and important impact on the electrical characteristics of crystalline boundaries, particularly in gas sensing [41].To assess the properties of the sensor concerning oxidizing gases, we examine the reaction of the MgO: SnO_2 samples to CO_2. When comparing the CO_2 response of MgO and SnO2 at different amounts and temperatures, it was found that at a temperature range of RT-200 °C, SnO_2 films exhibited a maximum CO_2 response of 9.75%.

In contrast, pure MgO and MgO $_{(0.5)}$: SnO_2 $_{(0.5)}$ films did not show such a high CO_2 response. Metal oxides with n-type conductivity, such as TiO_2, SnO_2, and ZnO, exhibit increased electrical resistance when exposed to gas [42]. It was observed in all samples that the recovery time values were greater than the response time. The gas molecules take time to release from the surface samples.

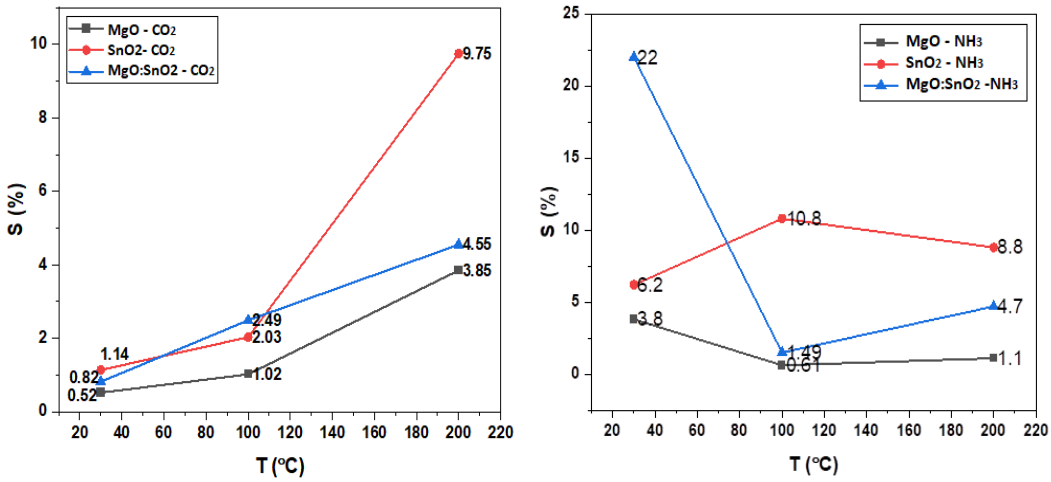

Fig. 6. CO_2 and NH_3 gas sensitivity for MgO, SnO_2 and $MgO_{(0.25)}$:$SnO_{2\ (0.25)}$ nanoparticles.

Table 2. Sensitivity, response time, and recovery time for MgO, SnO_2, and $MgO_{(0.5)}$: $SnO_{2\ (0.5)}$ Nanoparticles at different temperatures operating against CO_2 and NH_3 gases.

Gas type	CO2			NH3		
Sample no.	MgO Nanoparticles					
T (°C)	RT	100	200	RT	100	200
Sensitivity S %	0.52	1.02	3.85	3.8	0.61	1.1
Time res. ts (sec)	14	30	30	39	36	38
Time rec. tc (sec)	32	33	22	49	24	43
Sample no.	SnO2 Nanoparticles					
T (°C)	RT	100	200	RT	100	200
Sensitivity S %	1.14	2.03	9.75	6.2	10.8	8.8
Time res. ts (sec)	47	26	28	48	22	12
Time rec. tc (sec)	32	33	14	35	19	21
Sample no.	MgO: SnO2 Nanoparticles					
T (°C)	RT	100	200	RT	100	200
Sensitivity S %	0.82	2.49	4.55	22	1.49	4.7
Time res. ts (sec)	14	26	39	25	26	16
Time rec. tc (sec)	35	38	26	21	56	15

4. Conclusions

The results of the study are considered important for pollutant concentration detection. The size of the nanoparticles reduces as more MgO is added, and the nanoparticles have a complete rutile structure. The Hall Effect analysis revealed a modification in the conduction type from n-type to the most optimal resistivity of n-conductivity type 5.90 was achieved for SnO2 Pure.

The study focused on analysing NH3 and CO2 detection using drop-casted MgO: SnO2 thin films. The MgO: SnO2 films exhibited a more consistent sensing behavior and fully restored the baseline resistance, in contrast to the unmixed MgO, SnO2 films. The improvement in sensing capabilities of the MgO: SnO2 films is due to a reduction in crystallite size and an increase in defects, according to an increase in nanoparticle concentration. The data indicate that this significant enhancement is likewise linked to the production of MgO. Both the reduction in size and the inclusion of MgO have a significant role in enhancing the sensing behavior of MgO: SnO2 towards NH3.

References

[1] S. R. Gawali, V. L. Patil, V. G. Deonikar, S. S. Patil, D. R. Patil, P. S. Patil, J. Pant, Journal of Physics and Chemistry of Solids, **114**, 28–35 (2018); http://dx.doi.org/10.1016/j.jpcs.2017.11.005
[2] X. Liu, N. Chen, B. Han, X. Xiao, G. Chen, I. Djerdj, Y. Wang, Nanoscale, **7**(36), 14872–14880 (2015); http://dx.doi.org/10.1039/C5NR03585F
[3] R. Tian, P. Ji, Z. Luo, J. Li, J. Sun, New Journal of Chemistry, **45**(23), 10240–10247 (2021); http://dx.doi.org/10.1039/D1NJ01139A
[4] S. Giddey, S. P. S. Badwal, A. Kulkarni, International Journal of Hydrogen Energy, **38**, 14576–14594 (2013); https://doi.org/10.1016/j.ijhydene.2013.09.004
[5] B. Timmer, W. Olthuis, A. Van Den Berg, Sensors and Actuators B: Chemical, **107**, 666–677 (2005); https://doi.org/10.1016/j.snb.2004.11.054.
[6] D. Kwak, Y. Lei, R. Maric, Talanta, **204**, 713–730 (2019); https://doi.org/10.1016/j.talanta.2019.06.034
[7] R. H. Ayoub, M. H. AL-Timimi, M. Z. Abdullah, East European Journal of Physics, **3**, 546–554 (2023).
[8] H. S. Al-Rikabi, M. H. Al-Timimi, I. K. Abd, in AIP Conference Proceedings, **2834**, 1 (2023, December); https://doi.org/10.1063/5.0161779
[9] V. K. S. Yadav, T. T. Daniel, R. P. Paily, IEEE Sensors Journal, **20**, 4951–4958 (2020); http://dx.doi.org/10.1109/JSEN.2020.2966409
[10] M. Z. Abdullah, H. M. Hasan, M. H. Al-Timimi, W. H. Albanda, M. K. Alhussainy, M. Dumitru, Journal of Ovonic Research, **15**(3), 199–204 (2019).
[11] Z. Camtakan, S. Erenturk, S. Yusan, Environmental Progress & Sustainable Energy, **31**, 536–543 (2012); http://dx.doi.org/10.1002/ep.10569
[12] Z. Zhao, H. Dai, Y. Du, J. Deng, L. Zhang, F. Shi, Materials Chemistry and Physics, **128**, 348–356 (2011); http://dx.doi.org/10.1016/j.matchemphys.2011.03.013
[13] M. Sundararajan, J. Suresh, R. Rajiv Gandhi, Digest Journal of Nanomaterials and Biostructures, **7**, 983–989 (2012); https://doi.org/10.15251/DJNB.2012.73.983
[14] S. S. H. Al-Mgrs, M. H. Al-Timimi, M. Z. Abdullah, W. H. Al-Banda, in AIP Conference Proceedings, **2475**(1) (2023, March); http://dx.doi.org/10.1063/5.0103349
[15] R. V. Poonguzhali, E. R. Kumar, T. Pushpagiri, A. Steephen, N. Arunadevi, S. Baskoutas, Solid State Communications, **325**, 114161 (2021); http://dx.doi.org/10.1016/j.ssc.2021.114161
[16] F. R. Saeed, M. H. A. A. Al-Timimi, W. H. A. Al-Banda, M. Z. Abdullah, I. Stamatin, S. Voinea, A. E. Balan, Journal of Ovonic Research, **14**(5) (2018).
[17] C. Wang, J. Xu, B. Yang, F. Xia, Y. Zhu, J. Xiao, Solid-State Electronics, **147**, 19–25 (2018); https://doi.org/10.1016/j.esci.2022.02.008
[18] M. H. Al-Timimi, W. H. Albanda, M. Z. Abdullah, East European Journal of Physics, **2**, 173–181 (2023); https://doi.org/10.26565/2312-4334
[19] S. Shao, H. Wu, S. Wang, Q. Hong, R. Koehn, T. Wu, W. F. Rao, Journal of Materials Chemistry C, **3**(41), 10819–10829 (2015); http://dx.doi.org/10.1039/C5TC02400A
[20] D. Nunes, A. Pimentel, A. Gonçalves, S. Pereira, R. Branquinho, P. Barquinha, R. Martins, Semiconductor Science and Technology, **34**(4), 043001 (2019); http://dx.doi.org/10.1088/1361-6641/ab06d4

[21] A. Sharma, M. Tomar, V. Gupta, Sensors and Actuators B: Chemical, **156**, 743–752 (2019); https://doi.org/10.1016/j.snb.2011.02.026
[22] A.J. Mawat, M.H. Al-Timimi, W.H. Albanda, M.Z. Abdullah, AIP Conf. Proc., **2475**, 1 (2023); https://doi.org/10.1063/5.0172794
[23] C.M. Ghimbeu, M. Lumbreras, M. Siadat, R.C. van Landschoot, J. Schoonman, Sens. Actuat. B, **133**, 694 (2008); http://dx.doi.org/10.1016/j.snb.2008.04.003
[24] S.S. Chiad, N.F. Habubi, W.H. Abass, M.H. Abdul-Allah, J. Optoelectron. Adv. M. **18**, 822 (2016).
[25] K. Jain, R.P. Pant, S.T. Lakshmikumar, Sens. Actuat. B: Chemical, **113**, 823–829 (2006); http://dx.doi.org/10.1016/j.snb.2005.03.104
[26] H.S. Al-Rikabi, M.H. Al-Timimi, W.H. Albanda, Digest J. Nanomater. Biostruct., **17**, 3 (2022); https://doi.org/10.15251/DJNB.2022.173.889
[27] S. Vadivel, G. Rajarajan, J. Mater. Sci. Mater. Electron., **26**, 3155–3162 (2015); http://dx.doi.org/10.1007/s10854-015-2812-y
[28] C.I. Priyadharsini, M. Sumathi, A. Prakasam, P.M. Anbarasan, R. Sathiyapriya, V. Aroulmoji, Int. J. Adv. Sci. Eng., **3**, 428–434 (2017); http://dx.doi.org/10.1007/s12648-023-02714-y
[29] W.A. Aelawi, S. Alptekin, M.H. Al-Timimi, Indian J. Phys., **97**, 3949–3956 (2023); https://doi.org/10.1007/s12648-023-02736-6
[30] L.J.Q. Maia, C.R. Ferrari, V.R. Mastelaro, A.C. Hernandez, A. Ibanez, Solid State Sci., **10**, 1935 (2008); http://dx.doi.org/10.1016/j.solidstatesciences.2008.03.013
[31] Y.C. Liang, Y. Chao, Nanomaterials, **9**, 864 (2019); https://doi.org/10.3390/nano9060864
[32] J.B. Bult, R. Crisp, C.L. Perkins, J.L. Blackburn, ACS Nano, **7**, 7251–7261 (2013); https://doi.org/10.1021/nn402468e
[33] D. Kim, K.Y. Lee, M.K. Gupta, S. Majumder, S.W. Kim, Adv. Funct. Mater., **24**, 6949–6955 (2014); https://doi.org/10.1002/adfm.201401070
[34] A.T. Abood, O.A.A. Hussein, M.H. Al-Timimi, M.Z. Abdullah, H.M.S. Al Aani, W.H. Albanda, AIP Conf. Proc., **2213**, 1 (2020); https://doi.org/10.1063/5.0000284
[35] H.F. Haneef, A.M. Zeidell, O.D. Jurchescu, J. Mater. Chem. C, **8**, 759–787 (2020); https://doi.org/10.1039/C9TC05717C
[36] R. Wu, Y. Yu, S. Jia, C. Zhou, O. Cojocaru-Mirédin, M. Wuttig, Nat. Commun., **14**, 719 (2023); https://doi.org/10.1038/s41467-023-36281-y
[37] A. Valla, P. Carroy, F. Ozanne, D. Muñoz, Sol. Energy Mater. Sol. Cells, **157**, 874–880 (2016); https://doi.org/10.1016/j.solmat.2016.08.008
[38] K.K. Ato et al., J. Appl. Phys., **43**, 2311–2314 (2004); https://doi.org/10.1143/JJAP.43.2311
[39] S. Deshpande, D. Radhakrishnan, Sensors, **2**, 185–194 (2002); https://doi.org/10.3390/s20500185
[40] J.C. Hsieh, C.J. Liu, Y.H. Ju, Thin Solid Films, **322**, 98–103 (1998); https://doi.org/10.1016/S0040-6090(02)01180-9
[41] N. Yamazoe, K. Shimanoe, in Semiconductor Gas Sensors, Woodhead Publishing, pp. 3–38 (2020); https://doi.org/10.1016/B978-0-08-102390-1.00001-0
[42] A. Rydosz, W. Maziarz, A. Brudnik, A. Czapla, K. Zakrzewska, Proc. XV Int. Sci. Conf. Optoelectron. Electron. Sensors (COE), (2018); https://doi.org/10.1109/COE.2018.00021